Applications of Mathematics

Alexandros Markopoulos; Petr Beremlijski; Oldřich Vlach; Marie Sadowská Solution of 3D contact shape optimization problems with Coulomb friction based on TFETI

Applications of Mathematics, Vol. 68 (2023), No. 4, 405-424

Persistent URL: http://dml.cz/dmlcz/151702

Terms of use:

© Institute of Mathematics AS CR, 2023

Institute of Mathematics of the Czech Academy of Sciences provides access to digitized documents strictly for personal use. Each copy of any part of this document must contain these *Terms of use*.



This document has been digitized, optimized for electronic delivery and stamped with digital signature within the project $\mathit{DML-CZ}$: The Czech Digital Mathematics Library http://dml.cz

SOLUTION OF 3D CONTACT SHAPE OPTIMIZATION PROBLEMS WITH COULOMB FRICTION BASED ON TFETI

ALEXANDROS MARKOPOULOS, Evry, PETR BEREMLIJSKI, OLDŘICH VLACH, MARIE SADOWSKÁ, Ostrava

Received June 2, 2022. Published online December 6, 2022.

Dedicated to the memory of our friend Alexandros Markopoulos.

Abstract. The present paper deals with the numerical solution of 3D shape optimization problems in frictional contact mechanics. Mathematical modelling of the Coulomb friction problem leads to an implicit variational inequality which can be written as a fixed point problem. Furthermore, it is known that the discretized problem is uniquely solvable for small coefficients of friction. Since the considered problem is nonsmooth, we exploit the generalized Mordukhovich's differential calculus to compute the needed subgradient information.

The state problem is solved using successive approximations combined with the Total FETI (TFETI) method. The latter is based on tearing the bodies into "floating" subdomains, discretization by finite elements, and solving the resulting quadratic programming problem by augmented Lagrangians.

The presented numerical experiments demonstrate our method's power and the importance of the proper modelling of 3D frictional contact problems. The state problem solution and the sensitivity analysis process were implemented in parallel.

Keywords: shape optimization; nonsmooth optimization; contact problem; Coulomb's friction; TFETI method

MSC 2020: 65K10, 74M10, 65K05

DOI: 10.21136/AM.2022.0124-22 405

This work was partially supported by the European Regional Development Fund in "A Research Platform focused on Industry 4.0 and Robotics in Ostrava Agglomeration" project, Reg. No. $CZ.02.1.01/0.0/0.0/17_049/0008425$ within the Operational Programme Research, Development and Education. Further, this work was partially supported by the Ministry of Education, Youth and Sports of the Czech Republic through the e-INFRA CZ (ID:90140). This work was also partially supported by Grant of SGS No. SP2022/6 and No. SP2022/42, VSB-TU Ostrava.

1. Introduction

Shape optimization in contact mechanics aims to find shapes of deformable bodies, possibly in mutual contact. An essential feature of contact shape optimization with Coulomb's friction is its nonsmooth character, since the respective control-state mapping is typically nondifferentiable. To solve this problem correctly, one must use a special minimization method developed for nonsmooth optimization. More details can be found in [2], [1], [3], [16]. Note that not many papers deal with solving contact shape optimization problems, especially with friction. For example, the articles [15], [20] have been published in recent years in this area. In [15], the solution of the shape optimization problem for a frictionless contact problem is considered, which leads to a much easier optimization problem than we present in this paper. In [20], the shape and topological optimization problems with Coulomb friction are formulated and solved using regularization and penalization, leading to a simpler problem.

An efficient solution to contact problems is crucial in contact shape optimization applications in mechanical engineering. Large multibody contact problems of linear elastostatics, see, e.g., [6], are complicated due to the inequality boundary conditions. Moreover, if we admit "floating" bodies, the corresponding stiffness matrices are only positive semidefinite (i.e., singular). It is natural to assume that the solution of contact problems is more costly than that of a related linear problem with the classical Dirichlet and Neumann boundary conditions. For detailed information about our contact problem formulation approach and used minimization algorithms, see [7].

Let us point out that this article extends in many ways the brief conference paper [4]. Here, we again use Signorini and Hertz contact problems as academic benchmarks for the numerical experiments. However, these are now solved with significantly finer discretizations. This is achieved by speeding up the sensitivity analysis process, i.e., the computation of the Clarke subgradient, which is ensured using the Total FETI (TFETI) approach (see Section 4 and [6], [17]). Another substantial improvement is the parallelization of the state problem solution and also the parallel implementation of the sensitivity analysis. The experiments were carried out on the research infrastructure of IT4Innovations—the Czech National Supercomputing Center. Another aim of the paper is to show the significance of Coulomb's friction model, which has to be used for a sufficiently accurate solution of the problem leading to a homogeneous distribution of normal contact stress on the contact boundary (see Example 5.3).

The outline of the paper is as follows. In Section 2, we briefly present a formulation of the discrete state contact problem with Coulomb's friction by using the well-known TFETI. Section 3 focuses on the discrete shape optimization. In Section 4, we deal

with the computation of Clarke's subgradients of the respective locally Lipschitz and semismooth composite objective function that have to be supplied to the used algorithm of nonsmooth optimization. Section 5 is devoted to several test examples.

2. Setting of the discrete state problem

Here we present the algebraic setting of the discrete two-body contact problem with respect to the shape design variable α . In this section, all matrices and vectors (except \mathbf{f} , $F^{[2]}$, and \mathbf{c}_E) depend on the shape variable, so for the sake of lucidity we will omit this dependency in our notation. In Section 5, we test shape optimization

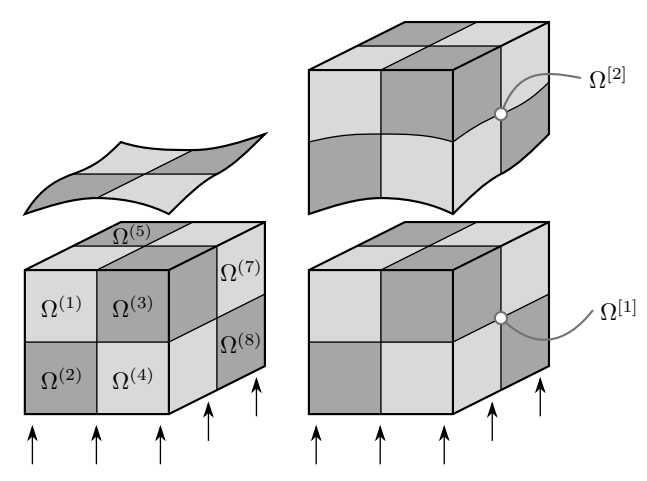


Figure 1. Contact problem types: body and rigid obstacle (left), two bodies (right). In this case, each body is decomposed into $2 \times 2 \times 2$ subdomains, i.e., n = 2.

on two types of 3D contact problems. The first type considers only one body in possible contact with rigid obstacle (see Fig. 1 left) and the second type is a two-body frictional contact problem (see Fig. 1 right). For reasons of clarity, we present here only the algebraic formulation of the more general setting—the two-body problem:

(2.1)
$$\mathbf{u}^* := \underset{\mathbf{u} \in \mathbb{R}^{3m}}{\min} J_h(\mathbf{u})$$
 subject to $\mathsf{N}\mathbf{u} \leqslant \mathbf{c}_N$ and $\mathsf{B}_E\mathbf{u} = \mathbf{c}_E$,

where m is the number of all nodes and

(2.2)
$$J_h(\mathbf{u}) := f(\mathbf{u}) + j_h(\mathbf{u}), \quad f(\mathbf{u}) := \frac{1}{2} \mathbf{u}^\top \mathsf{K} \mathbf{u} - \mathbf{u}^\top \mathbf{f},$$

and

$$\mathbf{u} = \begin{bmatrix} \mathbf{u}^{[1]} \\ \mathbf{u}^{[2]} \end{bmatrix}, \quad \mathsf{K} = \begin{bmatrix} \mathsf{K}^{[1]} & \mathsf{O} \\ \mathsf{O} & \mathsf{K}^{[2]} \end{bmatrix}, \quad \mathbf{f} = \begin{bmatrix} \mathbf{f}^{[1]} \\ \mathbf{f}^{[2]} \end{bmatrix}.$$

The upper indices ()^[1] and ()^[2] indicate the lower and upper body, respectively (see Fig. 1 right). Notice that for each $\Omega^{[i]}$, i=1,2, the vector $\mathbf{u}^{[i]}$ contains the displacements (in all three coordinate directions), $K^{[i]}$ is the stiffness matrix, $\mathbf{f}^{[i]}$ represents the load vector. Furthermore, N denotes the normal displacement jump matrix, \mathbf{c}_N is an initial gap, and \mathbf{B}_E with \mathbf{c}_E represent linear constraints stemming from both Dirichlet boundary condition and domain decomposition. The objective functional J_h is defined in (2.2) as the sum of f and f, which are the terms corresponding to the elastic and frictional energy, respectively. The frictional term f is described further in (2.3).

We consider our two-body contact problem with the following bodies and contact interfaces:

$$\begin{split} &\Omega^{[1]} := \{(x_1, x_2, x_3) \in (0, a) \times (0, b) \times \mathbb{R} \colon \ 0 < x_3 < F_{\pmb{\alpha}}^{[1]}(x_1, x_2)\}, \\ &\Omega^{[2]} := \{(x_1, x_2, x_3) \in (0, a) \times (0, b) \times \mathbb{R} \colon \ F^{[2]}(x_1, x_2) < x_3 < k\}, \\ &\Gamma_c^{[1]} := \{(x_1, x_2, F_{\pmb{\alpha}}^{[1]}(x_1, x_2)) \in [0, a] \times [0, b] \times \mathbb{R}\}, \\ &\Gamma_c^{[2]} := \{(x_1, x_2, F^{[2]}(x_1, x_2)) \in [0, a] \times [0, b] \times \mathbb{R}\}, \end{split}$$

where $F^{[2]}$ represents a given (fixed) shape of $\Gamma_c^{[2]}$ and $F_{\alpha}^{[1]}$ is a function extracting the upper boundary $\Gamma_c^{[1]}$ of the lower body $\Omega^{[1]}$ from shape design variable α . Notice that the upper side of the body $\Omega^{[2]}$ is flat, i.e., it is given by a constant k. In Fig. 1 we also illustrate that we utilized the domain decomposition technique to enable dealing with large domains. Thus, each $\Omega^{[i]}$ is decomposed into nonoverlapping subdomains $\Omega^{(j)}$,

$$\overline{\Omega^{[1]}} = \bigcup_{j=1}^{n^3} \overline{\Omega^{(j)}}, \quad \overline{\Omega^{[2]}} = \bigcup_{j=n^3+1}^{2n^3} \overline{\Omega^{(j)}},$$

where n stands for the number of subdomains in each coordinate direction and the line over a domain indicates its closure. We utilize TFETI (which stems from the original FETI [8]) for solving the state problem, where the Dirichlet boundary condition is imposed by Lagrange multipliers; see [6]. Torn subdomains are glued together by equality constraints using the matrix B_G and the Dirichlet conditions are treated in the same manner using the matrix B_D :

$$\mathsf{B}_E \mathbf{u} = \mathbf{c}_E, \quad \mathsf{B}_E := \begin{bmatrix} \mathsf{B}_G \\ \mathsf{B}_D \end{bmatrix}, \quad \mathbf{c}_E := \begin{bmatrix} \mathbf{c}_G \\ \mathbf{c}_D \end{bmatrix}.$$

The frictional term j_h in the case of Tresca friction is given using Lagrange multipliers λ_T as

(2.3)
$$j_h(\mathbf{u}) := \sum_{i=1}^{m_c} \Psi_i \| \mathsf{T}_i \mathbf{u} \| = \sum_{i=1}^{m_c} \max_{\|\boldsymbol{\lambda}_{Ti}\| \leqslant \Psi_i} \boldsymbol{\lambda}_{Ti}^\top \mathsf{T}_i \mathbf{u},$$

where Ψ_i is a given slip bound and m_c is the number of nodes on the contact boundary $\Gamma_c^{[1]}$. In (2.1) we use the α -dependent rows of the matrix N that extract normal jumps of the displacement between the boundaries $\Gamma_c^{[1]}$ and $\Gamma_c^{[2]}$. In the same manner, we introduce two-row tangential jump matrices T_i in (2.3). These matrices usually depend not only on the design variable α but also on the solution \mathbf{u}^* . In this text, we simplify our work and analysis by neglecting the dependence on \mathbf{u}^* and defining the outer normal only as the direction of the x_3 -axis.

Finally, let us introduce the algebraic formulation of our state *contact problem* with Tresca friction as

$$(\mathbf{u}^*, \boldsymbol{\lambda}^*) := \underset{\mathbf{u}}{\arg\min} \underset{\boldsymbol{\lambda}}{\sup} \mathcal{L}(\boldsymbol{\alpha})(\mathbf{u}, \boldsymbol{\lambda}_N, \boldsymbol{\lambda}_T, \boldsymbol{\lambda}_E) \text{ subject to } \boldsymbol{\lambda}_N \geqslant \mathbf{0} \text{ and } \|\boldsymbol{\lambda}_{Ti}\| \leqslant \Psi_i$$

with

$$\mathscr{L}(\boldsymbol{\alpha})(\mathbf{u},\boldsymbol{\lambda}_N,\boldsymbol{\lambda}_T,\boldsymbol{\lambda}_E) := f(\mathbf{u}) + \boldsymbol{\lambda}_T^\top \mathsf{T} \mathbf{u} + \boldsymbol{\lambda}_N^\top (\mathsf{N} \mathbf{u} - \mathbf{c}_N) + \boldsymbol{\lambda}_E^\top (\mathsf{B}_E \mathbf{u} - \mathbf{c}_E).$$

Here the Lagrange multipliers $\lambda := (\lambda_N, \lambda_T, \lambda_E)$ are marked with subscripts denoting normal, tangent, and equality parts, respectively.

Coulomb's friction. Finally, let us deal with the contact problem with Coulomb's friction and denote the coefficient of friction by \mathcal{F} . The Tresca friction can be utilized to define the mapping

$$\Xi \colon (\mathbb{R}_0^+)^{m_c} \mapsto (\mathbb{R}_0^+)^{m_c}, \quad \Xi(\mathbf{\Psi}) := \mathcal{F} \boldsymbol{\lambda}_N,$$

where \mathbb{R}_0^+ denotes all nonnegative real numbers. It can be shown that the fixed point of Ξ equals to the solution to the problem with Coulomb's friction. Here Ψ is a vector with the entries Ψ_i introduced in (2.3). It is well known [6], [21] that the sequence $\{\mathcal{F}\lambda_N^k\}$, $\mathcal{F}\lambda_N^{k+1} = \Xi(\mathcal{F}\lambda_N^k)$ with the initial slip bound $\mathcal{F}\lambda_N^0 \in (\mathbb{R}_0^+)^{m_c}$, converges to the fixed point $\mathcal{F}\lambda_N$ if the mapping Ξ is contractive in $(\mathbb{R}_0^+)^{m_c}$. In addition, such a fixed point exists uniquely provided \mathcal{F} is small enough. We also recommend the book [7] for further reading.

3. Discrete shape optimization

In the preceding section, we fixed the shape of the contact boundary. From now on, we will start using α as a design variable that controls our state problem. Let us denote by \mathcal{S} the *control-state mapping* that assigns the design variable $\alpha \in \mathbb{R}^d$ the solution (\mathbf{u}, λ) of the 3D contact problem with Coulomb's friction. Notice that $\mathcal{S}(\alpha)$ is nonempty for all $\alpha \in \mathcal{U}$, where \mathcal{U} is a set of all admissible design variables, and

single-valued for small friction coefficients. See [1] for details. Let us introduce a differentiable function

$$\mathcal{J}\colon\operatorname{Gr}\mathcal{S}\mapsto\mathbb{R}$$

that will be called an *objective function*. The term Gr S denotes the graph of S.

We will now establish the notation utilized in the following sections. If $\mathbf{F} \colon \mathbb{R}^p \mapsto \mathbb{R}^q$ is a Lipschitz single-valued mapping, then

$$\partial \mathbf{F}(\mathbf{x}) = \operatorname{conv} \left\{ \lim_{k \to \infty} \nabla \mathbf{F}(\mathbf{x}_k) \colon \mathbf{x}_k \overset{\Omega_F}{\to} \mathbf{x} \right\}$$

defines the generalized Jacobian of Clarke. The set Ω_F contains all points at which \mathbf{F} is differentiable. For q=1 the term $\partial \mathbf{F}(\mathbf{x})$ is the Clarke generalized gradient. Furthermore, we will use the following notions of Mordukhovich's generalized differential calculus [12], [13], [14]. If $A \subset \mathbb{R}^p$ is closed and a point $\overline{\mathbf{x}}$ belongs to A, then

$$\widehat{N}_A(\overline{\mathbf{x}}) = \left\{ \mathbf{x}^* \in \mathbb{R}^p \colon \limsup_{\mathbf{x} \xrightarrow{A} \overline{\mathbf{x}}} \frac{\langle \mathbf{x}^*, \mathbf{x} - \overline{\mathbf{x}} \rangle}{\|\mathbf{x} - \overline{\mathbf{x}}\|} \leqslant 0 \right\}$$

is the Fréchet regular normal cone to A at $\overline{\mathbf{x}}$. We define the limiting Mordukhovich normal cone to A at $\overline{\mathbf{x}}$ by

$$N_A(\overline{\mathbf{x}}) := \operatorname{Lim} \sup_{\mathbf{x} \xrightarrow{A} \overline{\mathbf{x}}} \widehat{N}_A(\mathbf{x}),$$

where "Lim sup" denotes the Kuratowski-Painlevé outer limit of sets; see [18]. If A is convex, then $N_A(\overline{\mathbf{x}}) = \widehat{N}_A(\overline{\mathbf{x}})$. Furthermore, we say that A is normally regular at $\overline{\mathbf{x}}$ if $N_A(\overline{\mathbf{x}}) = \widehat{N}_A(\overline{\mathbf{x}})$ holds true.

Based on the above definitions, let us describe the local behaviour of multifunctions. Let $\Phi \colon \mathbb{R}^p \rightrightarrows \mathbb{R}^q$ be a multifunction with a closed graph and let $(\overline{\mathbf{x}}, \overline{\mathbf{y}}) \in \operatorname{Gr} \Phi$. Then we define the multifunction $\widehat{D}^*\Phi(\overline{\mathbf{x}}, \overline{\mathbf{y}}) \colon \mathbb{R}^q \rightrightarrows \mathbb{R}^p$ as

$$\widehat{D}^*\Phi(\overline{\mathbf{x}},\overline{\mathbf{y}})(\mathbf{y}^*) := \{\mathbf{x}^* \in \mathbb{R}^p \colon (\mathbf{x}^*, -\mathbf{y}^*) \in \widehat{N}_{\mathrm{Gr}\,\Phi}(\overline{\mathbf{x}},\overline{\mathbf{y}})\}.$$

We call the above multifunction a regular coderivative of Φ at $(\overline{\mathbf{x}}, \overline{\mathbf{y}})$. The multifunction $D^*\Phi(\overline{\mathbf{x}}, \overline{\mathbf{y}}) \colon \mathbb{R}^q \rightrightarrows \mathbb{R}^p$ given by

$$D^*\Phi(\overline{\mathbf{x}},\overline{\mathbf{y}})(\mathbf{y}^*) := \{\mathbf{x}^* \in \mathbb{R}^p \colon \left(\mathbf{x}^*, -\mathbf{y}^*\right) \in N_{\operatorname{Gr}\Phi}(\overline{\mathbf{x}},\overline{\mathbf{y}})\}$$

is called a *limiting Mordukhovich coderivative* of Φ at $(\overline{\mathbf{x}}, \overline{\mathbf{y}})$. These two coderivatives are identical provided $\operatorname{Gr}\Phi$ is normally regular at the point $(\overline{\mathbf{x}}, \overline{\mathbf{y}})$. If Φ is single-valued, we simply write $\widehat{D}^*\Phi(\overline{\mathbf{x}})$ or $D^*\Phi(\overline{\mathbf{x}})$. Moreover, if Φ is continuously differentiable, then $\widehat{D}^*\Phi(\overline{\mathbf{x}}) = D^*\Phi(\overline{\mathbf{x}})$.

Now let us introduce the discrete optimal shape design problem as:

(3.1) Find
$$\mathbf{z}^* := (\boldsymbol{\alpha}^*, \mathbf{u}^*, \boldsymbol{\lambda}^*) \in \operatorname{Gr} \mathcal{S}$$
 such that $\mathcal{J}(\mathbf{z}^*) \leqslant \mathcal{J}(\mathbf{z}) \quad \forall \mathbf{z} \in \operatorname{Gr} \mathcal{S}$.

If \mathcal{F} is sufficiently small, then \mathcal{S} is single-valued and (3.1) can be written as:

(3.2) Find
$$\alpha^* \in \mathcal{U}$$
 such that $\Theta(\alpha^*) \leq \Theta(\alpha) \quad \forall \alpha \in \mathcal{U}$

with $\Theta(\alpha) := \mathcal{J}(\alpha, \mathcal{S}(\alpha))$. Observe that the control-state mapping \mathcal{S} is nondifferentiable, and therefore, the composite function $\Theta := \mathcal{J} \circ (I, \mathcal{S})$ is nondifferentiable as well.

To solve the shape optimization problem (3.2) we utilize our Matlab implementation of the bundle trust method. This method, which is very robust and well suited for minimizing nondifferentiable (nonsmooth) functions, is developed by combining the bundle and the trust region approaches; see [19] for more details. This iterative method needs a value of the objective function and one arbitrary Clarke subgradient at each step (see [5]), i.e., for each admissible α we must solve the state problem $(\mathbf{u}, \lambda) = \mathcal{S}(\alpha)$ and also compute a Clarke subgradient. Notice that finding a Clarke subgradient is the primary goal of Section 4.

The scheme of the blocks of the iterative process utilizing the bundle trust method for the solution of the shape optimization is depicted in Fig. 2.

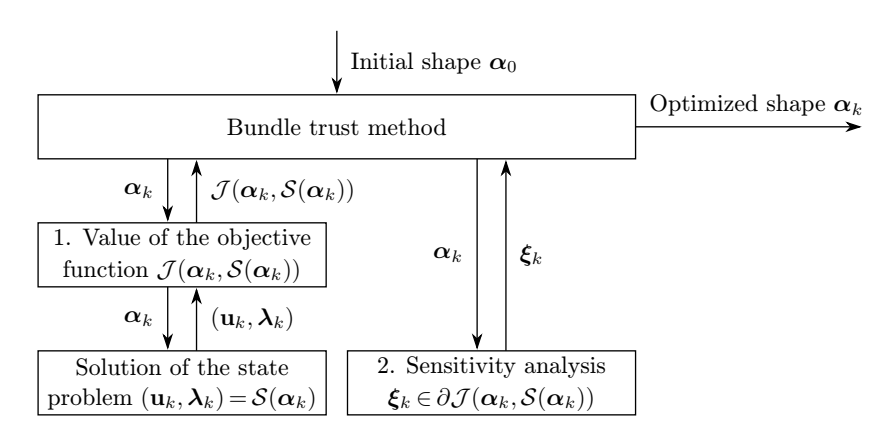


Figure 2. Block scheme of the shape optimization process with α_k denoting the vector of the shape variables and $\boldsymbol{\xi}_k$ denoting Clarke's subgradient (see Section 4).

Although a detailed description of the bundle trust method is not the aim of this paper, let us only briefly present a convergence result concerning minimization of a nonconvex, nonsmooth, locally Lipschitz, and weakly semismooth function f.

Recall that a function $f \colon \mathbb{R}^p \to \mathbb{R}$ is weakly semismooth if it is Lipschitz near all $\mathbf{x} \in \mathbb{R}^p$ and for all $\mathbf{x} \in \mathbb{R}^p$ there exists the limit

$$\lim_{\mathbf{g} \in \partial f(\mathbf{x} + t\mathbf{h}) \atop t \downarrow 0} \{ \langle \mathbf{g}, \mathbf{h} \rangle \} \quad \forall \, \mathbf{h} \in \mathbb{R}^p.$$

Theorem 3.1. If the function $f: \mathbb{R}^p \to \mathbb{R}$ is weakly semismooth, bounded below and the sequence of iterations $\{\mathbf{x}_k\}_{k\in\mathbb{N}}$ generated by the bundle trust method is bounded, then there exists a cluster point $\overline{\mathbf{x}} \in \mathbb{R}^p$ of the sequence $\{\mathbf{x}_k\}_{k\in\mathbb{N}}$ such that $\mathbf{0} \in \partial f(\overline{\mathbf{x}})$.

For more details, see [19]. Let us note that the used objective functions in Section 5 are locally Lipschitz and weakly semismooth. Thus, the existence of a cluster point $\overline{\mathbf{x}}$ for each objective function satisfying the condition $\mathbf{0} \in \partial f(\overline{\mathbf{x}})$ is guaranteed.

4. Sensitivity analysis

The aim of the sensitivity analysis is to compute one arbitrary Clarke subgradient (i.e., one element of the Clarke generalized gradient) of the objective function for each $\alpha \in \mathcal{U}$. To achieve this, in this section, we will use the definition of the Clarke generalized gradient and the limiting Mordukhovich coderivative introduced in Section 3.

The locally Lipschitz control-state mapping $S(\alpha)$ can be transformed into the following system of generalized equations:

(4.1)
$$\begin{cases} \mathbf{0} = \mathsf{K}_{f}(\boldsymbol{\alpha})\mathbf{u} - \mathbf{f}_{f}(\boldsymbol{\alpha}) - \mathsf{B}(\boldsymbol{\alpha})_{f}^{\top}\boldsymbol{\lambda}, \\ \mathbf{0} \in \mathsf{K}_{ct}(\boldsymbol{\alpha})\mathbf{u} - \mathbf{f}_{ct}(\boldsymbol{\alpha}) - \mathsf{B}(\boldsymbol{\alpha})_{ct}^{\top}\boldsymbol{\lambda} + \widetilde{Q}(\mathbf{u}_{ct}, \boldsymbol{\lambda}_{c}), \\ \mathbf{0} = \mathsf{K}_{c\nu}(\boldsymbol{\alpha})\mathbf{u} - \mathbf{f}_{c\nu}(\boldsymbol{\alpha}) - \mathsf{B}(\boldsymbol{\alpha})_{c\nu}^{\top}\boldsymbol{\lambda}, \\ \mathbf{0} \in \mathbf{c}(\boldsymbol{\alpha}) - \mathsf{B}(\boldsymbol{\alpha})_{c\nu}\mathbf{u} + N_{\mathbb{R}^{nc}_{c}}(\boldsymbol{\lambda}_{c}), \end{cases}$$

where the stiffness matrix K, the load vector \mathbf{f} , the matrix $\mathsf{B} := \mathsf{B}_E$, the displacements \mathbf{u} and the Lagrange multipliers $\boldsymbol{\lambda} := \boldsymbol{\lambda}_N$ are introduced in Section 2. The generalized equations (4.1) utilize the notation f for free nodes, c for contact nodes, t for tangential components, ν for normal components, $\mathbf{c}(\alpha)$ for the shape of contact boundary of the optimized body controlled by design variable α , and $N_{\mathbf{R}^p_+}$ for the standard normal cone; see [2]. Let us further define the multifunction \widetilde{Q} by

$$\widetilde{Q}(\mathbf{u}_{ct}, \boldsymbol{\lambda}_c) := \partial_{\mathbf{u}_t} j(\mathbf{u}_t, \boldsymbol{\lambda}_c)$$

with the friction term

$$j(\mathbf{u}_t, \boldsymbol{\lambda}_c) := \mathcal{F} \sum_{i=1}^{m_c} \boldsymbol{\lambda}_c^i \|\mathbf{u}_t^i\|.$$

We rewrite (4.1) as

$$\mathbf{0} \in \mathsf{F}(\boldsymbol{\alpha})\mathbf{y} - \boldsymbol{\ell}(\boldsymbol{\alpha}) + Q(\mathbf{y})$$

with

$$\begin{aligned} \mathbf{y} &:= (\mathbf{u}, \boldsymbol{\lambda})^{\top} \in \mathbb{R}^{3m+m_c}, \\ \mathsf{F}(\boldsymbol{\alpha}) &:= \begin{bmatrix} \mathsf{K}(\boldsymbol{\alpha}) & -\mathsf{B}(\boldsymbol{\alpha})^{\top} \\ -\mathsf{B}(\boldsymbol{\alpha}) & \mathsf{O} \end{bmatrix}, \\ \boldsymbol{\ell}(\boldsymbol{\alpha}) &:= (\mathbf{f}(\boldsymbol{\alpha}), -\mathbf{c}(\boldsymbol{\alpha}))^{\top}, \\ Q(\mathbf{y}) &:= (\mathbf{0}, \widetilde{Q}(\mathbf{u}_{ct}, \boldsymbol{\lambda}_c), \mathbf{0}, N_{\mathbb{R}^{m_c}_+}(\boldsymbol{\lambda}_c))^{\top}. \end{aligned}$$

Now let us compute one (arbitrary) Clarke subgradient. Using the chain rule, one can write

$$\partial \Theta(\alpha) \ni \boldsymbol{\xi} = \nabla_1 \mathcal{J}(\alpha, \mathcal{S}(\alpha)) + \{ C^{\top} \nabla_2 \mathcal{J}(\alpha, \mathcal{S}(\alpha)) \colon C \in \partial \mathcal{S}(\alpha) \}.$$

Since for all $\mathbf{y}^* \in \mathbb{R}^q$ we have

$$D^*\mathcal{S}(\boldsymbol{\alpha})(\mathbf{y}^*) \neq \emptyset$$
 and $\operatorname{conv}(D^*\mathcal{S}(\boldsymbol{\alpha}))(\mathbf{y}^*) = \{C^{\top}\mathbf{y}^* \colon C \in \partial \mathcal{S}(\boldsymbol{\alpha})\},$

only one element of $D^*\mathcal{S}(\alpha)(\nabla_2 \mathcal{J}(\alpha, \mathcal{S}(\alpha)))$ needs to be computed. The elements can be found from the limiting (Mordukhovich) coderivative

$$D^*\mathcal{S}(\boldsymbol{\alpha})(\mathbf{y}^*) := \{\mathbf{x}^* \in \mathbb{R}^p \colon (\mathbf{x}^*, -\mathbf{y}^*) \in N_{\mathrm{Gr}\,\mathcal{S}}(\boldsymbol{\alpha})\}$$

by the following theorem.

Theorem 4.1. Consider the reference pair (α, \mathbf{y}) with $\alpha \in \mathcal{U}$ and $\mathbf{y} = \mathcal{S}(\alpha)$. Then for all $\mathbf{y}^* \in \mathbb{R}^q$ we have

$$D^*\mathcal{S}(\boldsymbol{\alpha})(\mathbf{y}^*) \subset (\nabla \mathsf{F}(\boldsymbol{\alpha}) \cdot \mathbf{y} - \nabla \boldsymbol{\ell}(\boldsymbol{\alpha}))^{\top} \mathcal{V},$$

provided V is the set of solutions v to the (limiting) adjoint generalized equation

$$\mathbf{0} \in \mathbf{y}^* + (\mathsf{F}(\boldsymbol{\alpha}))^{\top} \mathbf{v} + D^* Q(\mathbf{y}, -\mathsf{F}(\boldsymbol{\alpha}) \mathbf{y} + \boldsymbol{\ell}(\boldsymbol{\alpha}))(\mathbf{v}).$$

For further details, see [1], [4].

Finally, the generalized equations from the latter theorem can be rewritten algebraically in order to compute one (arbitrary) Clarke subgradient $\boldsymbol{\xi} \in \partial \Theta(\boldsymbol{\alpha}) \in \mathbb{R}^d$ as

$$\boldsymbol{\xi} = \nabla_1 \mathcal{J}(\boldsymbol{\alpha}, \mathcal{S}(\boldsymbol{\alpha})) + \mathbf{p}^\top (\nabla \mathsf{F}(\boldsymbol{\alpha}) \cdot \mathbf{y} - \nabla \boldsymbol{\ell}(\boldsymbol{\alpha})), \quad \Pi \cdot \mathbf{p} = -\nabla_2 \mathcal{J}(\boldsymbol{\alpha}, \mathcal{S}(\boldsymbol{\alpha})),$$

where

$$\Pi = \begin{bmatrix} \mathsf{K} & -\mathsf{B}^\top \\ -\mathsf{B} & \mathsf{O} \end{bmatrix} + \begin{bmatrix} \widetilde{\mathsf{Q}}_1 & \mathsf{O} \\ \widetilde{\mathsf{Q}}_2 & \mathsf{O} \end{bmatrix},$$

 \widetilde{Q}_1 and \widetilde{Q}_2 are symmetric and nonsymmetric, respectively. To solve the adjoint generalized equation, we utilized the GMRES algorithm. To speed up the search for the solution of the limiting adjoint generalized equation, we used the TFETI method; see [9]. In addition, to further accelerate the computation, the whole process was parallelized.

5. Numerical experiments

In this section, we report results of our numerical experiments—the Signorini and Hertz contact problems (see Examples 5.1 and 5.2). Since these problems can be reformulated as fixed-point problems, successive approximations are utilized for their solutions. Each iterative step is represented by a contact problem with given friction computed from the previous iteration. This can be solved by using the algorithm suggested in [10] or, alternatively, one can exploit the approach proposed in [11]. We implemented the techniques described in Sections 2–4 in Matlab. To solve every state problem and sensitivity analysis in parallel, we employed 128 computational cores. All the computations ran on the research infrastructure of IT4Innovations—the Czech National Supercomputing Center.

The contact boundary $\Gamma_c^{[1]}$ is modelled by the cubic spline function $F^{[1]}$, therefore, the design variable α is the vector of its control points. Now, let us define the shape optimization problem (the solution procedure of which utilizing the bundle trust method is described in detail in Section 3) using this type of design variables:

(5.1) Minimize
$$\mathcal{J}(\alpha, \mathcal{S}(\alpha))$$
 subject to $\alpha \in \mathcal{U}$,

where

$$\begin{split} \mathcal{U} := \Big\{ \pmb{\alpha} \in \mathbb{R}^{d_1 \times d_2} \colon \ C_0 \leqslant \pmb{\alpha}^{(i,j)} \leqslant F^{[2]}(x_1,x_2), \ i = 0,1,\dots,d_1, \ j = 0,1,\dots,d_2; \\ |\pmb{\alpha}^{(i+1,j)} - \pmb{\alpha}^{(i,j)}| \leqslant C_1 \frac{a}{d_1}, \ i = 0,1,\dots,d_1-1, \ j = 0,1,\dots,d_2; \\ |\pmb{\alpha}^{(i,j+1)} - \pmb{\alpha}^{(i,j)}| \leqslant C_1 \frac{b}{d_2}, \ i = 0,1,\dots,d_1, \ j = 0,1,\dots,d_2-1; \\ C_{21} \leqslant \operatorname{meas} \Omega(\pmb{\alpha}) \leqslant C_{22} \Big\}, \end{split}$$

 C_0 , C_1 , C_{21} , and C_{22} are given positive constants and the function $F^{[2]}$ is for the Signorini problem defined by (5.3) and for the Hertz problem by the function describing contact boundary of the upper body. The constants d_1 and d_2 stand for the numbers of the shape design variables in the x_1 and x_2 coordinate directions, respectively. Note that the first set of constraints ensures that

$$|F_{\alpha}^{[1]}(x_1, x_2)| \geqslant C_0$$

for all $(x_1, x_2) \in [0, a] \times [0, b]$. The second and third constraint sets take care of the slopes of $F_{\alpha}^{[1]}$ in the x_1 and x_2 coordinate directions. It is well known that provided the control points fulfil the above conditions, then

$$\left| \frac{\partial}{\partial x_k} F_{\alpha}^{[1]}(x_1, x_2) \right| \leqslant C_1$$

for all $(x_1, x_2) \in [0, a] \times [0, b]$ and k = 1, 2. The fourth constraint is given in order to control the domain's volume by the control points of the cubic spline, so that it determines the volume of the body

(5.2)
$$\Omega^{[1]}(\boldsymbol{\alpha}) := \{ (x_1, x_2, x_3) \in (0, a) \times (0, b) \times \mathbb{R} \colon 0 < x_3 < F_{\boldsymbol{\alpha}}^{[1]}(x_1, x_2) \}.$$

Example 5.1. Let us first consider a single elastic body in possible contact with a rigid obstacle; see Fig. 3. We look for a shape of the contact boundary minimizing the peak of normal contact stress that is represented by Lagrange multipliers $\lambda(\alpha)$, in other words, we want to find $\alpha \in \mathcal{U}$ that minimizes the max-norm of $\lambda(\alpha)$. Because the max-norm is not continuously differentiable, we utilize the p-norm $\|\cdot\|_p$ instead, taking p large enough (p := 4 in our case).

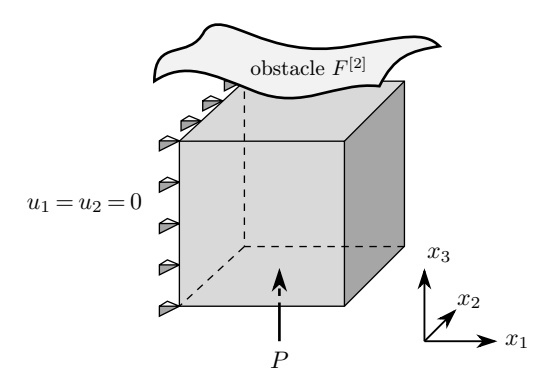


Figure 3. Example 5.1, setting of the problem.

The elastic body $\Omega^{[1]}(\alpha)$ is for any $\alpha \in \mathcal{U}$ determined by (5.2) with a:=100 mm and b:=100 mm. The set \mathcal{U} of all admissible designs is given by $C_0:=50$, $C_1:=5$, $C_{21}:=0.8\cdot 10^6$ mm³, and $C_{22}:=1.2\cdot 10^6$ mm³. The Dirichlet part of the boundary (with prescribed zero displacements in the x_1 and x_2 directions) is defined as $\Gamma_u^{[1]}:=\{(0,x_2,x_3)\in\overline{\Omega^{[1]}(\alpha)}\}$; see Fig. 3. Let us further define the nonzero external loads. The bottom face $\Gamma_P^{[1]}:=\{(x_1,x_2,0)\in\overline{\Omega^{[1]}(\alpha)}\}$ is subjected to the constant pressure $P:=3\cdot 10^3$ N/mm². The upper face $\Gamma_c^{[1]}$ modelled by $F_\alpha^{[1]}$ is constrained by the rigid obstacle $F^{[2]}$ given by

(5.3)
$$F^{[2]}(x_1, x_2) := \sin\left(\frac{2\pi x_1}{100}\right) + 2\cos\left(\frac{2\pi x_2}{100}\right) + 103$$

for all $(x_1, x_2) \in [0, a] \times [0, b]$. The elastic material parameters are as follows: the Young modulus $E := 1.1 \cdot 10^5$ MPa, Poisson's ratio $\sigma := 0.33$, and the friction coefficient $\mathcal{F} := 0.3$.

We are concerned with the shape optimization problem:

(5.4) Minimize
$$\mathcal{J}(\boldsymbol{\alpha}, \mathcal{S}(\boldsymbol{\alpha})) = \mathcal{J}(\boldsymbol{\alpha}, (\mathbf{u}, \boldsymbol{\lambda})) := \|\boldsymbol{\lambda}(\boldsymbol{\alpha})\|_4^4$$
 subject to $\boldsymbol{\alpha} \in \mathcal{U}$.

The elastic "cube" (see Fig. 3) was uniformly cut into $35 \times 35 \times 35 = 42\,875$ bricks. We also uniformly decomposed the body into $5 \times 5 \times 5 = 125$ subdomains and applied the finite element discretization using trilinear hexahedral elements. The total numbers of nodal displacements and design variables were 192 000 and 36, respectively, and the number of Lagrange multipliers was 1296.

In Fig. 4, the shape of the rigid obstacle can be seen.

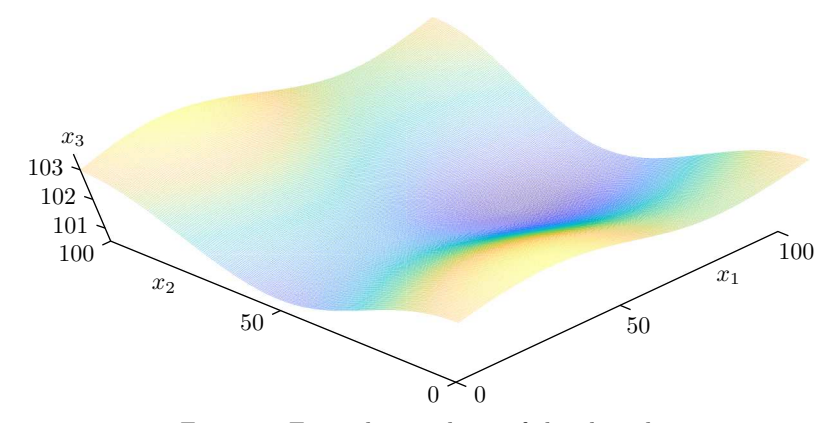


Figure 4. Example 5.1, shape of the obstacle.

The von Mises stress for the initial and otpimized shapes $\Omega^{[1]}(\boldsymbol{\alpha}_{in})$ and $\Omega^{[1]}(\boldsymbol{\alpha}_{opt})$ is shown in Fig. 5 on the left and on the right, respectively.

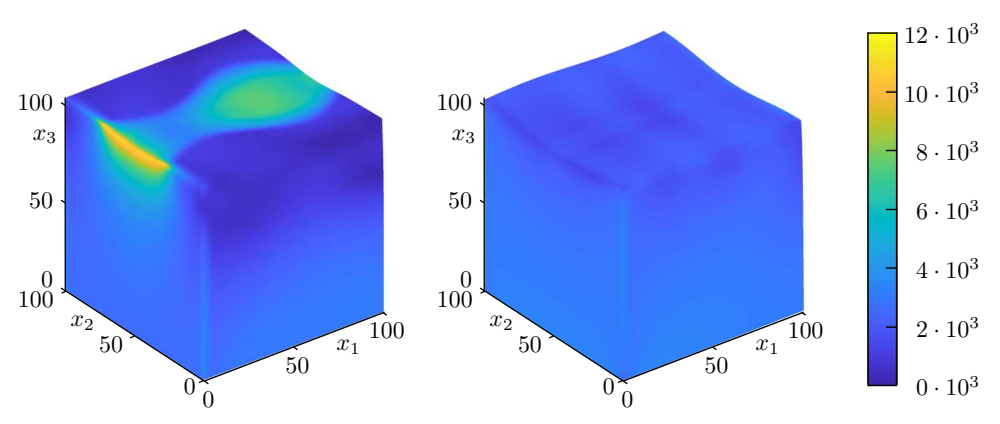


Figure 5. Example 5.1, von Mises stress for initial (left) and optimal (right) design.

Furthermore, in Fig. 6, we depict the normal contact stress along the contact part of $\Omega^{[1]}(\alpha_{\rm in})$ (left) and $\Omega^{[1]}(\alpha_{\rm opt})$ (right). We can see that the peak of stress is considerably suppressed and, in addition, the normal contact stress along the contact part of $\Omega^{[1]}(\alpha_{\rm opt})$ is evenly distributed. The values of the objective function at $\alpha_{\rm in}$ and $\alpha_{\rm opt}$ are $3.9691 \cdot 10^{18}$ and $1.1065 \cdot 10^{17}$, respectively.

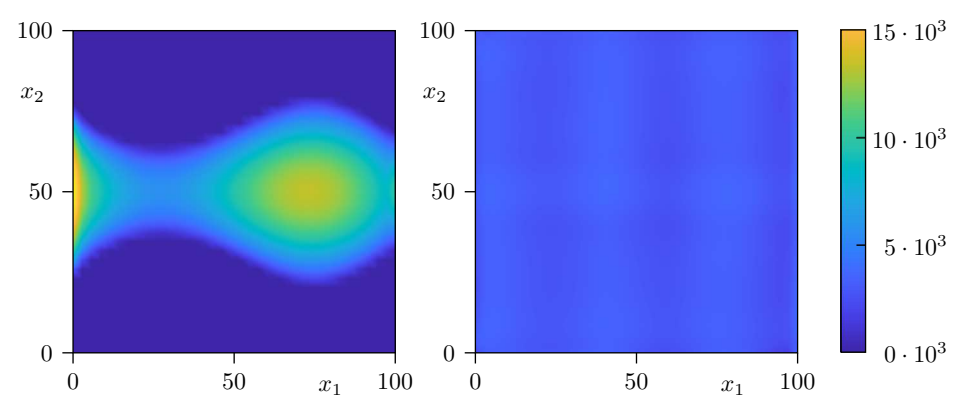


Figure 6. Example 5.1, normal contact stress for initial (left) and optimal (right) design.

Example 5.2. Now let us consider two elastic bodies in possible bilateral contact, see Fig. 7. Similarly to the previous example, we aim to find the shape of the lower body's contact boundary minimizing the peak of the normal contact stress represented by the Lagrange multipliers $\lambda(\alpha)$. In other words, we look for a minimizer $\alpha \in \mathcal{U}$ of the max-norm of $\lambda(\alpha)$. Moreover, due to the nondifferentiability of the max-norm, we again utilize the norm $\|\cdot\|_4$ instead.

The settings now slightly differ from those used in Example 5.1. The lower elastic body $\Omega^{[1]}(\boldsymbol{\alpha})$ is for an $\boldsymbol{\alpha} \in \mathcal{U}$ prescribed by (5.2) with a := 10 mm and b := 10 mm. The upper elastic body $\Omega^{[2]}$ is defined by

$$\Omega^{[2]} := \{ (x_1, x_2, x_3) \in (0, a) \times (0, b) \times \mathbb{R} \colon F^{[2]}(x_1, x_2) < x_3 < k \}$$

with a := 10 mm, b := 10 mm, k := 20 mm, and $F^{[2]}$ is given by

$$F^{[2]}(x_1, x_2) := 20 - \sqrt{20^2 - x_1^2 - x_2^2}.$$

The set \mathcal{U} of all admissible designs is defined by $C_0 := 5$, $C_1 := 5$, $C_{21} := 0.8 \cdot 10^3$ mm³, and $C_{22} := 1.2 \cdot 10^3$ mm³. We used these choices of the material parameters: the Young modulus $E := 7 \cdot 10^4$ MPa (or $E := 2.1 \cdot 10^5$ MPa) and Poisson's ratio $\sigma := 0.35$ (or $\sigma := 0.29$) for the lower (or upper) body, and the friction coefficient $\mathcal{F} := 0.3$.

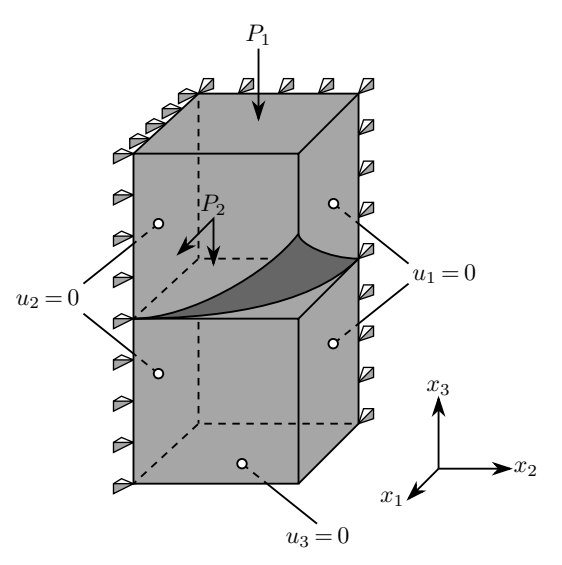


Figure 7. Example 5.2, setting of the problem.

We prescribe the density of surface tractions as $\mathbf{P}_1 := (0, 0, -2000 \text{ MPa})$ on the top of the upper body and $\mathbf{P}_2 := (500 \text{ MPa}, 0, -2000 \text{ MPa})$ on the front face of the upper body. Moreover, we impose zero normal displacements on the bottom of the lower body and on the left and right faces of both bodies. Let us consider the shape optimization problem:

(5.5) Minimize
$$\mathcal{J}(\alpha, \mathcal{S}(\alpha)) = \mathcal{J}(\alpha, (\mathbf{u}, \lambda)) := \|\lambda(\alpha)\|_4^4$$
 subject to $\alpha \in \mathcal{U}$.

Each of the elastic bodies (see Fig. 7) was uniformly cut into $25 \times 25 \times 25 = 15\,625$ bricks and uniformly decomposed into $5 \times 5 \times 5 = 125$ subdomains. We used trilinear hexahedral finite elements for the discretization. The total numbers of nodal displacements and design variables were 162 000 and 36, respectively. The number of Lagrange multipliers was 676. The lower body's contact boundary is modelled by a cubic spline, the shape of which is controlled by design variables.

The von Mises stress corresponding to the initial shape $\Omega^{[1]}(\boldsymbol{\alpha}_{in})$ and to the optimized shape $\Omega^{[1]}(\boldsymbol{\alpha}_{opt})$ is shown in Fig. 8 on the left and on the right, respectively.

Fig. 9 depicts how the normal contact stress is distributed along the contact part of $\Omega^{[1]}(\alpha_{\rm in})$ (left) and $\Omega^{[1]}(\alpha_{\rm opt})$ (right), respectively. It is seen that the peak of stress is again considerably suppressed. The values of the objective function at $\alpha_{\rm in}$ and $\alpha_{\rm opt}$ are $1.9255 \cdot 10^{18}$ and $2.2250 \cdot 10^{17}$, respectively.

Example 5.3 (Comparisons of the solutions of the contact shape optimization with and without friction). To see the importance of proper modelling of 3D contact problems with friction, let us deal with a problem similar to that of Example 5.1,

but now without friction. We aim to compare the solution of the Signorini problem with the nonzero friction coefficient $\mathcal{F} := 0.3$ (see Example 5.1) with the solution of the same problem with zero friction coefficient. Let us stress that the function $\Theta(\alpha) := \mathcal{J}(\alpha, \mathcal{S}(\alpha))$ is differentiable considering the friction coefficient equals to zero, therefore, its minimization is much simpler.

Let us consider the situation from Example 5.1 with the very same geometry and elastic material settings (see Fig. 3), the shape of the rigid obstacle (see Fig. 4), and the resulting shape optimization problem (5.4).

The elastic body was uniformly cut into $12 \times 12 \times 12 = 1728$ bricks and uniformly divided into $2 \times 2 \times 2 = 8$ subdomains. The trilinear hexahedral finite elements were utilized. The total numbers of nodal displacements and design variables were 8232 and 36, respectively, and the number of Lagrange multipliers was 169.

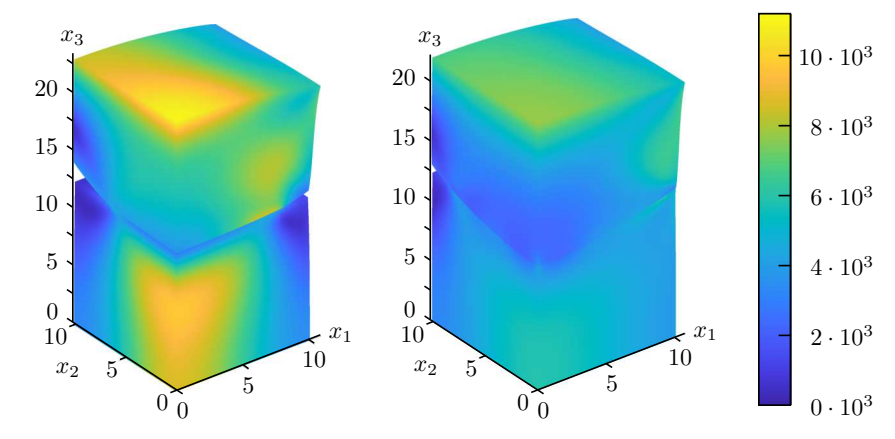


Figure 8. Example 5.2, von Mises stress for initial (left) and optimal (right) design.

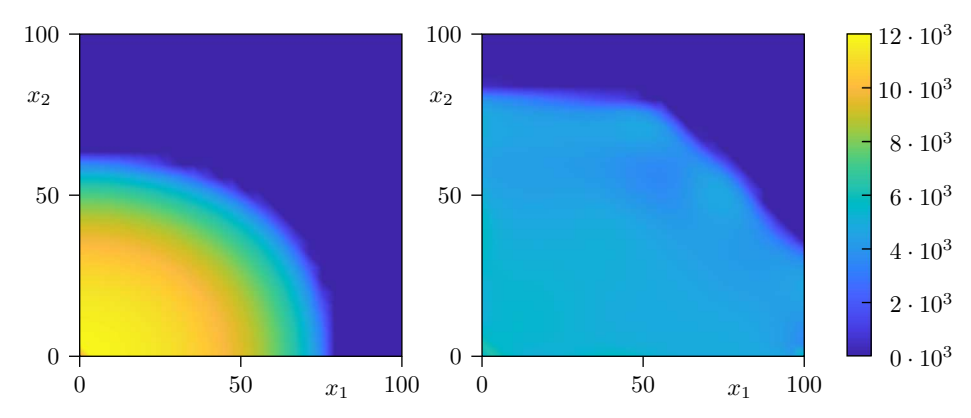


Figure 9. Example 5.2, normal contact stress for lower body of initial (left) and optimal (right) design.

The von Mises stress corresponding to the initial shape $\Omega^{[1]}(\boldsymbol{\alpha}_{in})$ and to the optimized shape $\Omega^{[1]}(\boldsymbol{\alpha}_{opt})$ is depicted in Figs. 10 and 11 for the friction coefficient $\mathcal{F} := 0.3$ and zero friction coefficient, respectively.

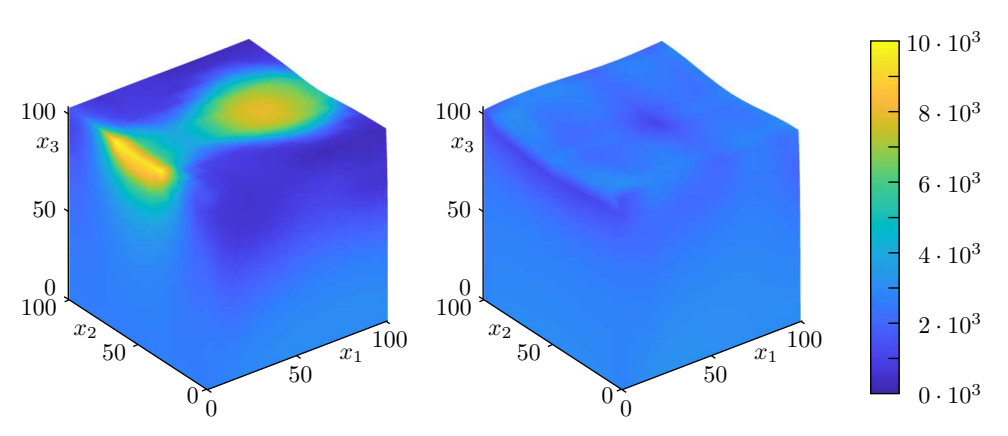


Figure 10. Example 5.3, von Mises stress for initial (left) and optimal (right) design (with friction).

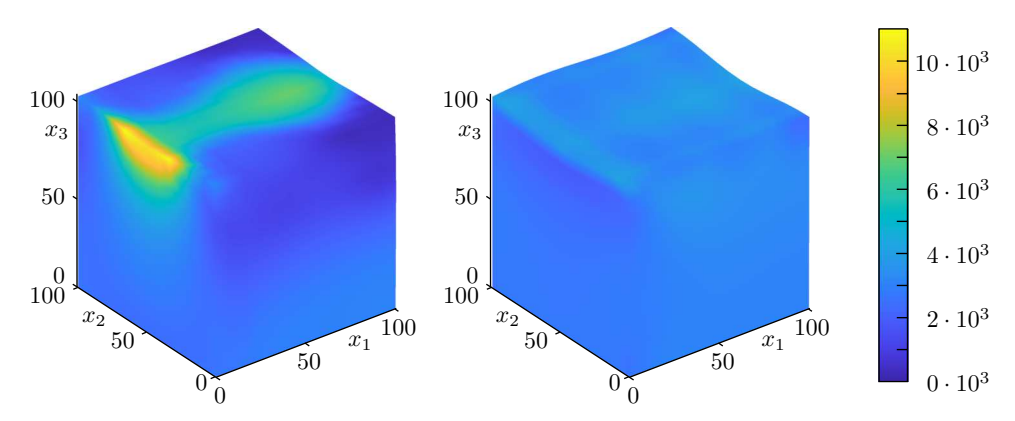


Figure 11. Example 5.3, von Mises stress for initial (left) and optimal (right) design (without friction).

Figs. 12 and 13 depict the distribution of the normal contact stress along the contact part of $\Omega^{[1]}(\boldsymbol{\alpha}_{\rm in})$ (left) and $\Omega^{[1]}(\boldsymbol{\alpha}_{\rm opt})$ (right) for the friction coefficient $\mathcal{F} := 0.3$ and zero friction coefficient, respectively. These figures show that the peak of stress is considerably suppressed and, in addition, the normal contact stress along the contact part of $\Omega^{[1]}(\boldsymbol{\alpha}_{\rm opt})$ is evenly distributed. Notice that the optimized shapes computed for the two previous friction coefficient choices are very similar.

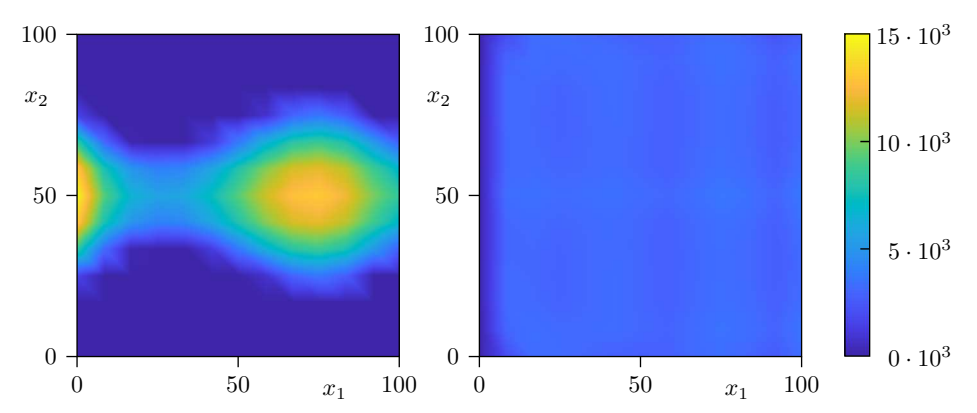


Figure 12. Example 5.3, normal contact stress for initial (left) and optimal (right) design (with friction).

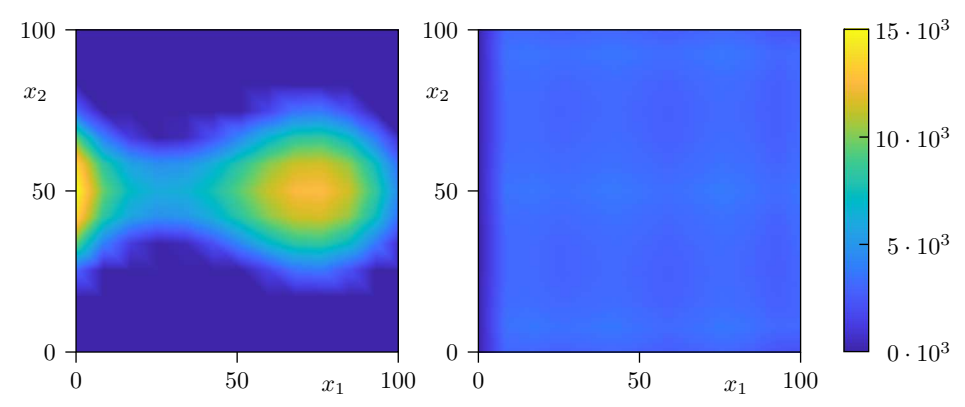


Figure 13. Example 5.3, normal contact stress for initial (left) and optimal (right) design (without friction).

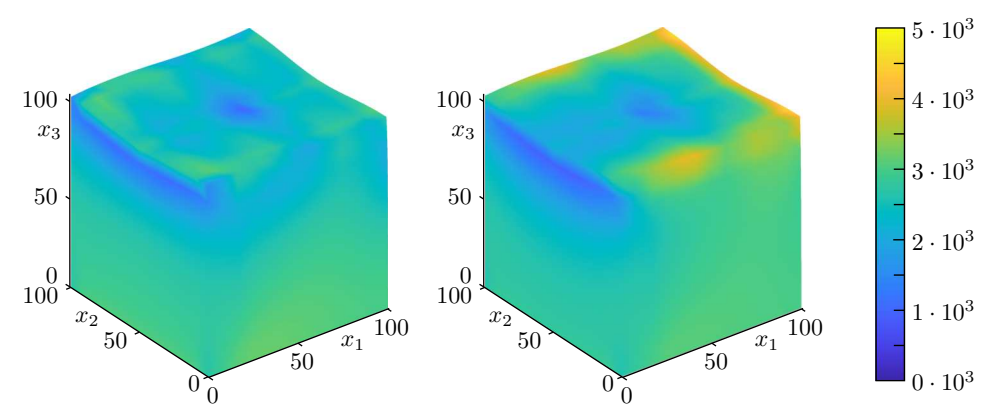


Figure 14. Example 5.3, comparison (both with friction): von Mises stress for optimized design computed for problem with nonzero friction coefficient (left) and zero friction coefficient (right).

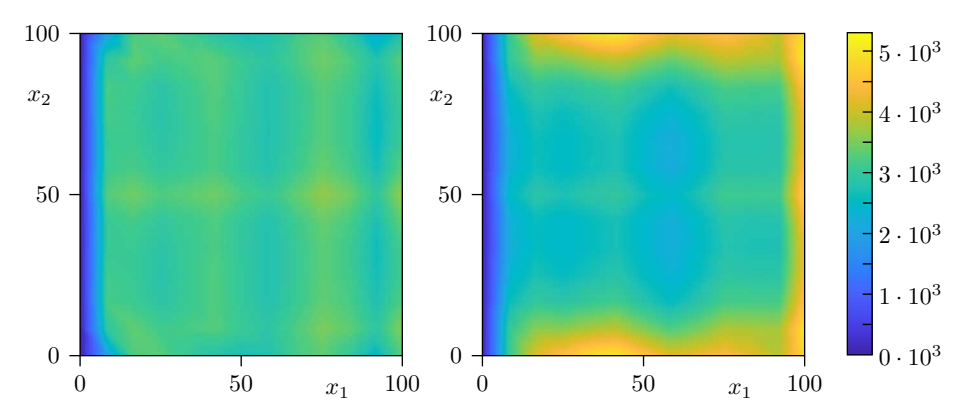


Figure 15. Example 5.3, comparison (both with friction): normal contact stress for optimized design computed for problem with nonzero friction coefficient (left) and zero friction coefficient (right).

Finally, let us compute two state problems with the friction coefficient $\mathcal{F} := 0.3$ and with different lower body shapes. In the first case, the lower body has the optimized shape for the computation with friction (see Fig. 10 right), and in the second case, the lower body has the optimized shape for the computation without friction (see Fig. 11 right). Figs. 14 and 15 show the comparisons of the von Mises stress and the normal contact stress for both problems, respectively. These figures show that replacing the Coulomb friction problem with a (much simpler) model without friction does not make much sense to get an "approximate optimal design".

6. Comments and conclusions

A method for the parallel solution of 3D shape optimization problems of contact mechanics with Coulomb's friction was presented. We had to deal with the fact that our problem was nonsmooth. We implemented the utilized bundle trust method in Matlab and used the Mordukhovich differential calculus for the sensitivity analysis. Moreover, the sensitivity analysis process was accelerated using TFETI. For the discretization and solution of the state contact problem, the TFETI approach and the augmented Lagrangians method combined with active set based algorithms were used, respectively. To speed up the whole solution process, we parallelized both the solution of the state contact problem and the sensitivity analysis. The efficiency of our approach was demonstrated on two academic benchmarks. Finally, we also stress the *importance of using frictional models* in 3D contact mechanics. Our method can be successfully applied to industrial problems modelled as 3D shape optimization problems of frictional contact mechanics since they typically need very fine discretizations.

References

[1]	P. Beremlijski, J. Haslinger, M. Kočvara, R. Kučera, J. V. Outrata: Shape optimization in three-dimensional contact problems with Coulomb friction. SIAM J. Optim. 20 (2009), 416–444.		MR do
[2]	P. Beremlijski, J. Haslinger, M. Kočvara, J. Outrata: Shape optimization in contact problems with Coulomb friction. SIAM J. Optim. 13 (2002), 561–587.	zbl	MR do
[3]	P. Beremlijski, J. Haslinger, J. V. Outrata, R. Pathó: Shape optimization in contact problems with Coulomb friction and a solution-dependent friction coefficient. SIAM	-h1	MD
	J. Control Optim. 52 (2014), 3371–3400. P. Beremlijski, A. Markopoulos: On solution of 3D contact shape optimization problems with Coulomb friction based on domain decomposition. EngOpt 2014 4th International Conference on Engineering Optimization. IDMEC - Instituto de Engenharia Mecanica, Lisboa, 2015, pp. 465–470. E. H. Charles Optimization and Nonremosth Applysis. Consider Methometical Society.	doi	MR do
	F. H. Clarke: Optimization and Nonsmooth Analysis. Canadian Mathematical Society Series of Monographs and Advanced Texts. John Wiley & Sons, New York, 1983. Z. Dostál, T. Kozubek, A. Markopoulos, T. Brzobohatý, V. Vondrák, P. Horyl: Theoret-	zbl	MR do
ĮΟJ	ically supported scalable TFETI algorithm for the solution of multibody 3D contact problems with friction. Comput. Methods Appl. Mech. Eng. 205-208 (2012), 110–120.	zbl	MR do
[7]	Z. Dostál, T. Kozubek, M. Sadowská, V. Vondrák: Scalable Algorithms for Contact Problems. Advances in Mechanics and Mathematics 36. Springer, New York, 2016.	zbl	MR do
[8]	C. Farhat, FX. Roux: An unconventional domain decomposition method for an efficient parallel solution of large-scale finite element systems. SIAM J. Sci. Stat. Comput. 13 (1992), 379–396.	zbl	MR do
[9]	J. Haslinger, T. Kozubek, R. Kučera, G. Peichl: Projected Schur complement method for solving non-symmetric systems arising from a smooth fictitious domain approach. Numer. Linear Algebra Appl. 14 (2007), 713–739.		MR do
[10]	$R.~Ku\check{c}era:$ Minimizing quadratic functions with separable quadratic constraints. Optim. Methods Softw. 22 (2007), 453–467.	zbl	MR do
[11]	R. Kučera, K. Motyčková, A. Markopoulos, J. Haslinger: On the inexact symmetrized globally convergent semi-smooth Newton method for 3D contact problems with Tresca friction: The R-linear convergence rate. Optim. Methods Softw. 35 (2020), 65–86.	zbl	MR do
[12]	B.S.Mordukhovich: Variational Analysis and Generalized Differentiation. I. Basic Theory. Grundlehren der Mathematischen Wissenschaften 330. Springer, Berlin, 2006.	zbl	MR doi
	B. S. Mordukhovich: Variational Analysis and Generalized Differentiation. II. Applications. Grundlehren der Mathematischen Wissenschaften 331. Springer, Berlin, 2006.	zbl	MR do
	B. S. Mordukhovich: Variational Analysis and Applications. Springer Monographs in Mathematics. Springer, Cham, 2018.	zbl	MR do
	 A. Myśliński: Topology optimization of elasto-plastic contact problems. AIP Conf. Proc. 2239 (2020), Article ID 020031, 2 pages. J. V. Outrata, M. Kočvara, J. Zowe: Nonsmooth Approach to Optimization Problems 	doi	
	with Equilibrium Constraints: Theory, Applications and Numerical Results. Nonconvex Optimization and Its Applications 28. Kluwer, Dordrecht, 1998.	zbl	MR doi
	L. Říha, T. Brzobohatý, A. Markopoulos: Hybrid parallelization of the total FETI solver. Adv. Eng. Softw. 103 (2017), 29–37.	doi	
	R. T. Rockafellar, R. JB. Wets: Variational Analysis. Grundlehren der Mathematischen Wissenschaften 317. Springer, Berlin, 1998.	zbl	MR do
[19]	H.Schramm,J.Zowe: A version of the bundle idea for minimizing a nonsmooth function: Conceptual idea, convergence analysis, numerical results. SIAM J. Optim. 2 (1992), 121–152.	zbl	MR do

[20] A. Sharma, R. Rangarajan: A shape optimization approach for simulating contact of elastic membranes with rigid obstacles. Int. J. Numer. Methods Eng. 117 (2019), 371–404.

Multidiscip. Optim. 42 (2010), 955-964.

- 371–404. MR doi
 [21] V. Vondrák, T. Kozubek, A. Markopoulos, Z. Dostál: Parallel solution of contact shape optimization problems based on total FETI domain decomposition method. Struct.
 - zbl MR doi

Authors' addresses: Alexandros Markopoulos, Safran Aircraft Engines, 10, allée du Brévent, 91019 Evry, France; Petr Beremlijski (corresponding author), Department of Applied Mathematics, VSB-Technical University of Ostrava, 17. listopadu 2172/15, 708 00 Ostrava-Poruba, Czech Republic, e-mail: petr.beremlijski@vsb.cz; Oldřich Vlach, Department of Applied Mathematics, VSB-Technical University of Ostrava, 17. listopadu 2172/15, 708 00 Ostrava-Poruba, Czech Republic and IT4Innovations National Supercomputing Center, VSB-Technical University of Ostrava, Studentská 6231/1B, 708 00 Ostrava-Poruba, Czech Republic, e-mail: oldrich.vlach2@vsb.cz; Marie Sadowská, Department of Applied Mathematics, VSB-Technical University of Ostrava, 17. listopadu 2172/15, 708 00 Ostrava-Poruba, Czech Republic, e-mail: marie.sadowska@vsb.cz.